Power budget analysis for waveguide-enhanced Raman spectroscopy

Zilong Wang[a*], Stuart J. Pearce[b], Yung-Chun Lin[c], Michalis N. Zervas[a], Philip N. Bartlett[c] and James S. Wilkinson[a]

[a]*Optoelectronics Research Centre, University of Southampton,* Southampton, SO17 1BJ UK

[b]*Electronics and Computer Science, University of Southampton,* Southampton, *SO17 1BJ UK*

[c]*Chemistry, University of Southampton,* Southampton, SO17 1BJ UK

*zw1e09@soton.ac.uk

Abstract

Waveguide-enhanced Raman spectroscopy (WERS) is emerging as an attractive alternative to plasmonic SERS approaches as it can provide more reproducible quantitative spectra on a robust chip without the need for nanostructured plasmonic materials. Realising portable WERS Raman systems with high sensitivity using low-cost laser diodes and compact spectrometers requires a detailed analysis of the power budget from laser to spectrometer chip. In this paper we describe theoretical optimisation of planar waveguides for maximum Raman excitation efficiency, demonstrate WERS for toluene on a silicon process compatible high index contrast tantalum pentoxide waveguide, measure the absolute conversion efficiency from pump power to received power in an individual Raman line, and compare this with a power budget analysis of the complete system including collection with an optical fibre and interfacing to a compact spectrometer. Optimised 110nm thick Ta_2O_5 waveguides on silica substrates excited at a wavelength of 637nm are shown experimentally to yield overall system power conversion efficiency of $\sim 0.5\times10^{-12}$ from the pump power in the waveguide to the collected Raman power in the 1002 cm^{-1} Raman line of toluene, in comparison with a calculated efficiency of 3.9×10^{-12}. Collection efficiency is dictated by the numerical and physical apertures of the spectral detection system but may be improved by further engineering the spatial and angular Raman scattering distributions.

Keywords:

Integrated Optics; Optical Waveguides; Waveguide Raman Spectroscopy; Surface Enhanced Raman Spectroscopy

1. Introduction

Raman spectroscopy is a powerful analytical technique yielding rich molecular information through the vibrational "fingerprint" of molecules, making it attractive for chemical sensing and biosensing applications. Fluorescence-based approaches, where electronic transition cross-sections are normally six to eight orders of magnitude larger than Raman cross-sections, resulting in much larger signal power, are the most widespread means of detection in biosensing applications [1]. However, in that case, the molecule of interest is usually tagged with a fluorophore and specificity is not obtained directly from the molecule but by binding to a receptor, requiring significant sample pre-treatment and expensive reagents. For reactions at surfaces, as in most biosensing approaches, surface-enhanced Raman spectroscopy (SERS) provides great surface selectivity and enhancement of Raman signal strength by a factor of typically $10^6 – 10^{10}$ [2], rendering it competitive with fluorescence techniques with the advantages of greater multiplexability (for SERS with fluorescent tags [3]) and potentially direct information on the molecular structure [4]. The realisation of repeatable SERS surfaces with large average enhancement factors is an extremely active field of research [5], but there are few examples of successful commercialisation [6]. The large enhancement is

mainly due to the electromagnetic mechanism provided by plasmonic structures made of noble metals such as gold. Difficulties in repeatably fabricating these structures with tolerances of a few nanometres, for SERS with the highest enhancement factors ($> 10^{10}$), lead to the need to compromise between enhancement and reproducibility.

Portability and low cost are important factors in achieving widespread *in-situ* use of biosensors, and this has driven the use of optical waveguides for biosensors using many different optical transduction phenomena. Monomode waveguide-based spectroscopy is, in effect, an optimised implementation of TIR spectroscopy [7], with maximised signal enhancement [8]. Optical waveguide devices offer excitation and collection light paths which do not pass through the sample under analysis, robustness, sensitivity, integration of on-chip multisensor arrays, potential for mass-production, and use of compact portable instrumentation, rather than expensive, fixed laboratory instruments. Examples of this approach applied to fluorescence-based multi-sensing include the AWACSS system [9] and the US NRL Array Biosensor system [10]. Dielectric waveguides themselves provide enhancement of electric fields at their surfaces, leading to what is referred to as waveguide-enhanced Raman spectroscopy (WERS) [11], without the advantages of optical localisation for greater surface selectivity and extreme local enhancement but also without the disadvantages of complex nanostructuring or of reduced repeatability and robustness. Waveguide-enhanced Raman spectroscopy (WERS) is emerging as a competitive analytical tool which avoids nanostructured noble metal surfaces but which potentially provides comparable average surface enhancements in a sensorised format [12,13].

Waveguides were first used to study Raman scattering of thin films where the film being studied formed the guiding core of the waveguide [14–18]. These were followed by several studies of resonance Raman scattering from monolayers on low index contrast glass or polymer waveguides [19]. While optimisation of waveguides for surface enhancement was not directly addressed, it was observed that enhancement of Raman excitation for thin films resulted from maintaining a high excitation intensity over an increased scattering volume of analyte [17]. Subsequently, an analysis of the intensity of the evanescent field at the surface of an optical waveguide emphasised that thin high-index waveguides yielded the greatest field enhancement for Raman excitation and this was demonstrated experimentally for both a 8 nm thick polystyrene film and a protein monolayer on an optimised high index contrast ZnO waveguide on SiO_2 [13]. The enhancement achieved by WERS may not be sufficient for single molecule detection [20] unless combined with other enhancement mechanisms such as plasmonics in nanostructured gold [11,21], but is very promising for analytical applications where more modest, but repeatable, surface average enhancements are required, such as biosensors employing surface reactions in ultrathin films.

There is renewed interest in utilising dielectric waveguides [12,22], silicon waveguides [23] or waveguides combined with plasmonic structures [11,24,25] for enhanced Raman spectroscopy, driven primarily by the need for large enhancement factors combined with improved repeatability. Comparison of these approaches would be aided by rigorous quantification of the power conversion efficiency from the laser pump to the Raman signal and of the enhancement of Raman signal compared to a conventional configuration. We present a theoretical and experimental analysis of a full WERS system, for the case of waveguide excitation and surface collection, as shown in Figure 1a, compared with conventional Raman illumination as shown in Figure 1b. A power budget analysis relates the received power in a single Raman scattering line to the incident pump laser power, using waveguide surface intensity and Raman cross-section. This approach allows straightforward WERS optimization and a clear comparison of surface-enhanced techniques.

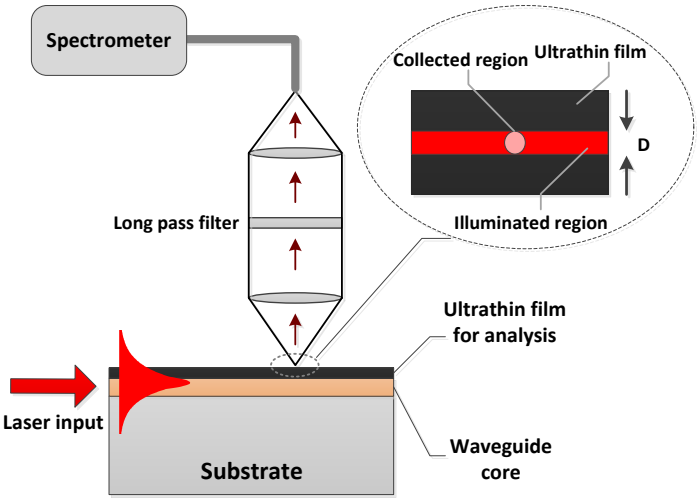

Figure 1a. Waveguide Raman excitation configuration with surface collection

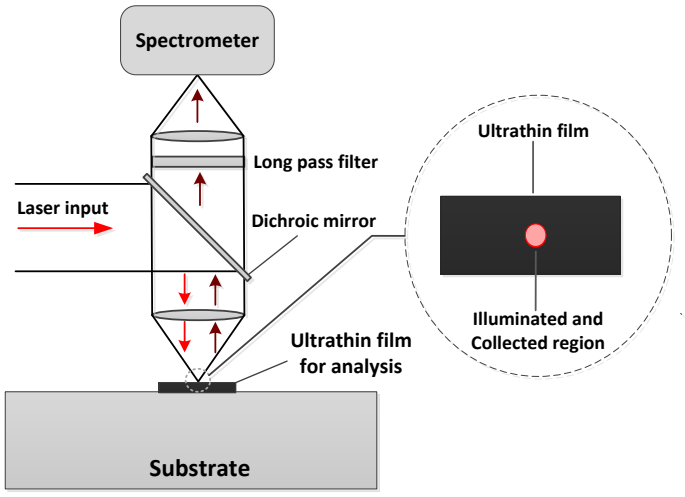

Figure 1b. Conventional Raman configuration

2. Design and simulation

In common with SERS, waveguide excitation of Raman scattering is determined by the magnitude of the electric field experienced by the Raman medium, so that the optimisation of devices for surface excitation consists of maximising the electric field from the laser "pump" at the location of the species of interest for a given pump power over a certain surface area. In SERS and waveguide collection configurations, the enhancement of Raman scattering and the signal collection efficiency are also determined by the local electric field distributions, but this may be strongly dependent upon the frequency (Stokes) shift of the Raman line [26]. The excitation enhancement in a waveguide geometry is first described in order to select the waveguide materials for this study. A pump wavelength of 637 nm has been chosen as a compromise between low fluorescence and the ability to detect large Stokes' shifts using a silicon CCD spectrometer, for ease of use, and for comparison with a conventional Raman instrument at a similar wavelength.

2.1 Waveguide surface intensity. For Raman spectroscopy of very thin layers, the key advantage of waveguide surface excitation (Fig 1a) over conventional excitation with a focussed beam perpendicular to the layer (Fig 1b) is that in one dimension (waveguide thickness), the intensity spot-size can be drastically reduced, and surface intensity thereby significantly increased, without any reduction in the irradiated surface area. In the case of conventional perpendicular excitation, the product of surface intensity and area is fixed (and approximately equal to the incident power). As a result, for thin layers the product of intensity and irradiated area can be much greater in the waveguide excitation case. In addition, in the waveguide case, the electromagnetic field falls exponentially as it penetrates into the analyte medium, with an 1/e intensity penetration depth of order 100 nm, making the waveguide an inherently surface sensitive technique that largely eliminates bulk media interference. While the product of intensity and irradiated volume should be optimised for sensitive analysis of bulk media, this reduces to maximising the product of intensity and area for very thin films, which is where waveguide excitation provides a significant advantage. To illustrate this, the intensity at the surface of a 1D (slab) dielectric waveguide, normalised to 1W modal power per metre waveguide width, I_n, has been calculated using a similar approach to Kanger et al. [10], and has units of m^{-1} due to the normalisation. Examples for the TE and TM polarised fundamental modes

are plotted in Figure 2a against waveguide core thickness for a wavelength of 637nm, substrate refractive index of $n_2 = 1.46$ (silica), superstrate refractive index of $n_3 = 1.33$ (water), for two core refractive indices $n_1 = 2.1$ (similar to Ta_2O_5 and Si_3N_4 [12]) and $n_1 = 1.53$ (Corning 7059 glass [19]). Ta_2O_5 and Si_3N_4 are both silicon process compatible dielectric materials transparent in the visible and near-infrared parts of the electromagnetic spectrum.

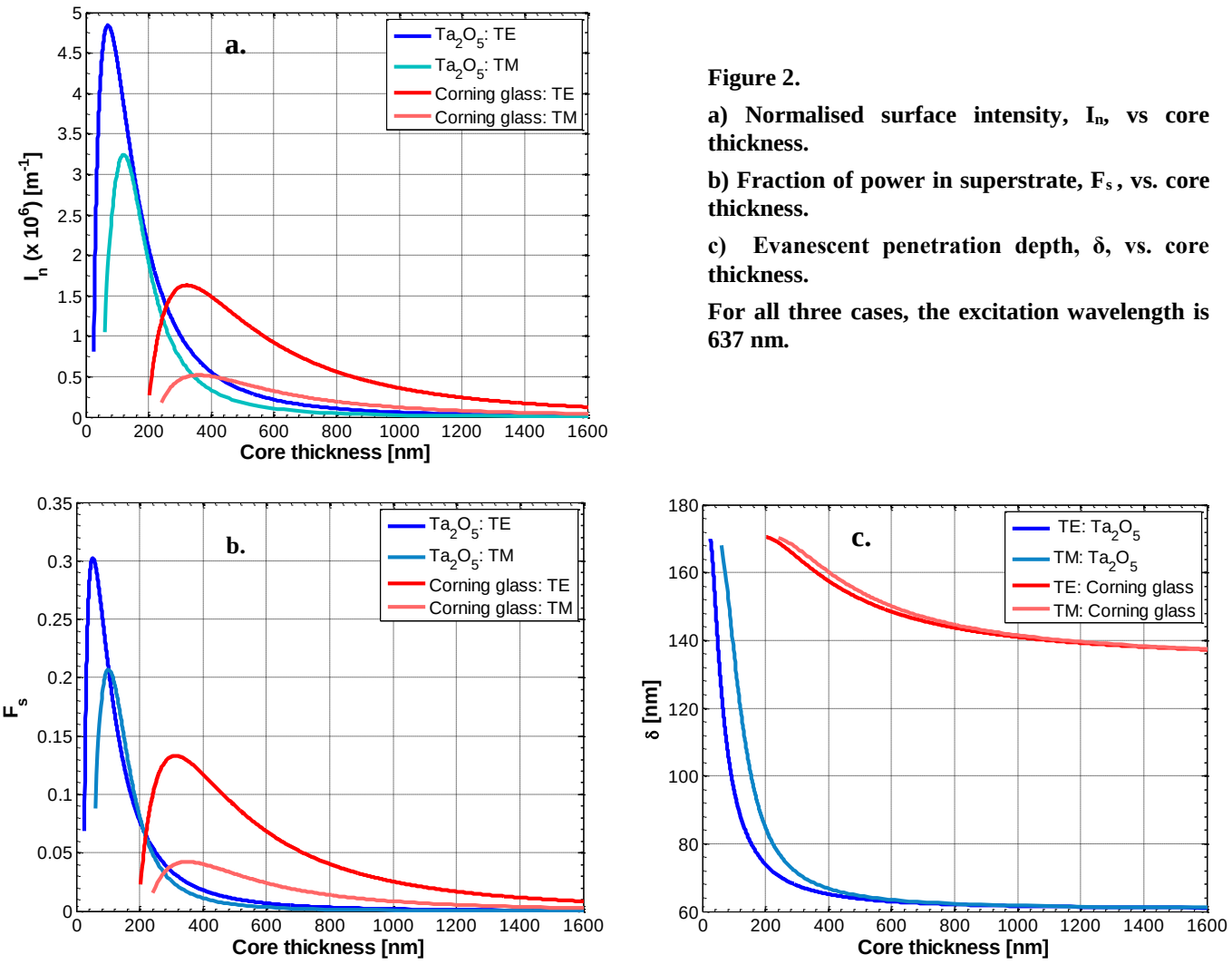

Figure 2.

a) Normalised surface intensity, I_n, vs core thickness.

b) Fraction of power in superstrate, F_s, vs. core thickness.

c) Evanescent penetration depth, δ, vs. core thickness.

For all three cases, the excitation wavelength is 637 nm.

CThe maximum normalised surface intensity, I_n, of ~ 4.8×10^6 m^{-1} occurs for the fundamental mode in the TE polarisation for the high index waveguide, as expected [13]. Assuming negligible waveguide loss and negligible pump depletion, for the same pump power, the resultant Raman excitation (the product of surface intensity and area) is I_n times greater than conventional excitation perpendicular to the thin film *per metre length of waveguide*. The maximum useful waveguide length is then defined by the collection configuration. This assumes insignificant pump depletion along the length of the waveguide, which is reasonable for lengths up to 1cm with losses typically of order 1 dB/cm for high contrast waveguides. Figure 2b shows the evanescent penetration depth vs. waveguide core thickness, which for a Ta_2O_5 waveguide takes the range 60 nm – 170 nm, corresponding to a mode far from and near to cutoff, respectively. Surface films with thickness of a few nm may thus be assumed to experience the surface intensity shown in Fig 2a. Figure 2c shows the fraction of power carried in the bulk superstrate (in this case water) by the waveguide mode,

F_s, for the same waveguide designs, showing similar behaviour to the surface intensity, modified slightly by the changing penetration depth. Waveguide Raman analysis of bulk media should be optimised using this parameter. For future comparisons with composite plasmonic structures, the TM polarisation was chosen for this study, and so a tantalum pentoxide film of thickness 110 nm on a 1 mm thick silica substrate was selected to be optimum.

2.2 Surface collection of Raman scattering. A conventional Raman microscope system focuses pump light onto the sample using a microscope objective lens and collects the emitted Raman signal through the same lens and directs it through filters to a spectrometer, as shown in Fig 1b. Increasing the numerical aperture (NA) of the lens reduces the spotsize of the incident power allowing higher spatial resolution but, for a uniform film under study, does not change the emitted Raman power (ignoring saturation effects). However, the increased NA does increase the efficiency of collection of the emitted power and, for isotropic emission, this follows:

$$\eta_c = 1/2 \times [1 - cos(sin^{-1}NA)] \quad (1)$$

In the case of waveguide excitation with surface normal collection, shown in Fig 1a, the collection optics can be optimised independently of the excitation optics, so that even if the surface intensity is no higher than for conventional Raman illumination, the emission can be collected over a larger area. For a low-cost system, where ultimate spectral resolution is not a requirement, the most practical configuration is to use a compact fibre-coupled CCD spectrometer. In this case the maximum collection efficiency is obtained with the collecting end of the fibre as close as possible to the emissive surface [27], using the NA of the fibre in Eqn 1. The maximum total collected power is then obtained by summing the contributions from all emitting molecules within the area of the fibre core. Thus the maximum efficiency is obtained by using the highest NA fibre with a core that covers the maximum length of the waveguide possible, while ensuring the width of the waveguide illumination, D, is confined to the width of the fibre core. In practice, a lens system imaging a region of the emissive surface onto the end of the collection fibre allows collection without contact between the fibre and surface and the placing of pump filters before the collection fibre, and will only marginally affect the collection efficiency due to additional reflections etc. For this study, we used a highly multimode 1 mm core diameter fibre with an NA of 0.48. Assuming isotropic emission, this is expected to yield a collection efficiency for an individual emitter of ~6.1%. To compare excitation using an optimised tantalum pentoxide waveguide to a conventional Raman instrument having a similar NA, if the waveguide illumination width is narrower than the fibre core then, from Fig 2, the collected power is expected to be ~4800 times larger, due to the 1 mm collection length. However, there will be a trade-off between spectral resolution and signal power at the fibre/spectrometer interface due to the use of a large high NA multimode fibre.

3. Materials and methods

The waveguide materials were selected to be SiO_2 for the substrate, due to its combination of low refractive index, low fluorescence, robustness and availability and Ta_2O_5 for high surface intensity as described above and low loss to allow long path length [28]. Both materials are compatible with silicon processing. The excitation wavelength was chosen to be 637 nm, to use a semiconductor laser, and the waveguide core thickness selected to be 110 nm to yield near-optimum surface intensity as described in Section 2.1. The waveguide was fabricated by RF sputtering onto a 50 mm square, 1 mm thick, silica substrate at a temperature of 200 ºC from a 150 mm diameter powder-pressed pure Ta_2O_5 target with power of 300 W,

oxygen flow of 5 sccm and argon flow of 20 sccm. The chamber was maintained at a pressure of 10 mTorr and the film was deposited at a rate of 3.42 nm/min over 32 min.

Raman scattering from bulk toluene (C_7H_8, n = 1.489) was chosen for this study and prism-coupling was used to excite the waveguide mode, for experimental convenience. While Raman spectroscopy from an ultrathin film would show the most advantage for WERS, the Raman cross-section of toluene is large and well known [29] and a robust comparison of theory and experiment can be readily performed by assuming that the evanescent field is filled with toluene. Validating the theory with a bulk medium also eliminates potential errors due to thickness tolerances and molecular alignment. A reference spectrum for the toluene (Sigma-Aldrich, anhydrous, 99.8%) was first taken with a conventional Raman instrument operating at 633 nm (Renishaw 2000) using a quartz cuvette. Light from a 637nm fibre-coupled semiconductor laser (Thorlabs LP637-SF70) was coupled into the waveguide sample using a microscope objective lens (Melles Griot ×10) and high-index prism (Metricon 200-P-2) as shown in Figure 3. TM polarisation was chosen for these measurements, and 44 mW power was incident on the prism in this polarisation. The use of a low-cost semiconductor laser would enable cheap portable high sensitivity Raman instrumentation where ultimate spectral resolution is not required.

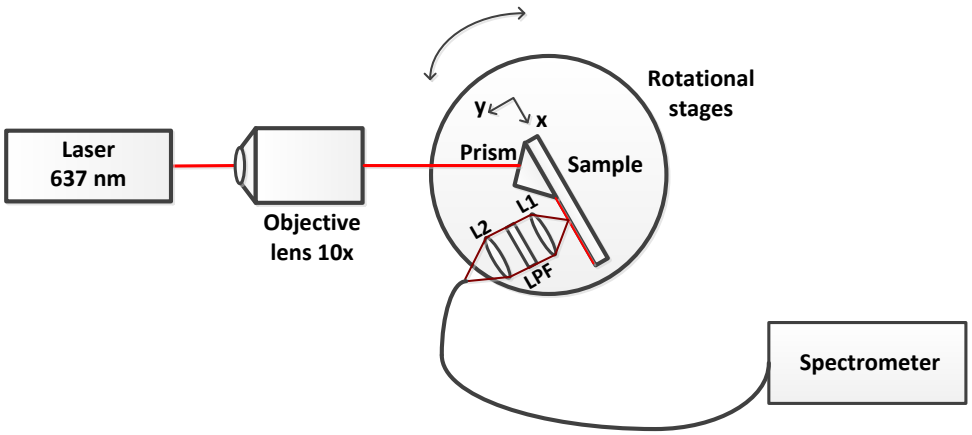

B2. Figure 3. Apparatus for waveguide Raman measurements. L1: convex lens with f=25.4 mm, diameter is 1 inch. L2: achromatic lens with f=30 mm, diameter is 1 inch. LPF: long pass filter for laser wavelength between 635 nm to 642 nm and the edge wavelength is 655 nm. The acquisition time is 60 s.

The Raman collection optics consisted of two 1 inch diameter lenses (L1: f=25.4 mm, L2: f=30 mm) coupling through a multimode fibre (NA: 0.48, Core diameter: 1 mm) into a compact spectrometer (Ocean Optics QE65000 Pro) with a 200 μm entrance slit. A long-pass filter (LPF, FELH0650 Thorlabs) with a band edge at 648 nm was placed between the lenses to suppress scattered pump radiation, cutting out signals with Stokes' shifts below 300 cm^{-1}. The spectrometer was USB interfaced to a PC and SpectraSuite software was used to control the spectrometer and process the data.

A small drop of toluene was placed onto the waveguide surface and a coverslip located on top to reduce evaporation. The penetration depth of the evanescent field into the toluene is approximately 120 nm and the resulting toluene layer fills this region, resulting in effectively a bulk analyte above the waveguide surface rather than the very thin film as encountered in biosensing. Nonetheless, this is sufficient to validate the design and confirm the power budget. The collection system was focussed onto the waveguide surface

approximately 2.5 cm away from the prism coupling position and spectra were recorded with an integration time of 60 s.

4. Results and Discussion

4.1 Raman spectra. The reference spectrum for toluene with baseline correction, taken using the conventional instrument, is shown in Figure 4a (grey trace) for comparison with the waveguide spectrum. The Raman scattering peak at 1002 cm^{-1} has a published differential Raman cross-section $d\sigma/d\Omega$ of $3.2\pm0.3 \times 10^{-30}$ cm^2/sr at a pump wavelength of 633 nm [29].

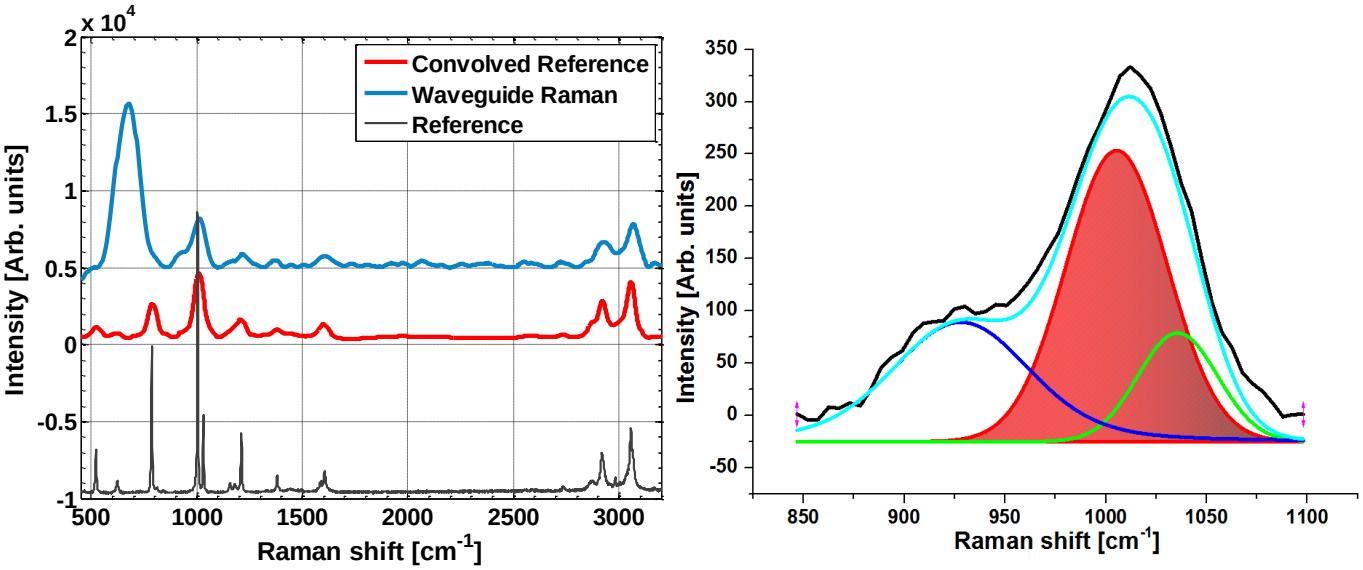

B3. Figure 4(a). Raman spectra of toluene: Black trace: Reference spectrum from conventional Raman instrument, Red trace: reference spectrum convolved with system spectral transfer function, Blue trace: waveguide Raman spectrum (The three traces are offset for clarity); (b) Voigt function peak fitting to the spectral features near 1000 cm^{-1}. The red, green and blue curves represent the toluene Raman peaks at 1002 cm^{-1} and 1029 cm^{-1}, and background from the silica substrate respectively

The prism coupling efficiency is estimated to be 30% and the Raman spectrum is collected from the waveguide surface at a position 2.5 cm after input coupling and with the estimated propagation loss of 2 dB/cm, the pump power in the waveguide at this position is estimated to be 4.4 mW. Figure 4a shows the Raman spectrum collected from the waveguide surface (blue trace), baseline corrected in the same way as the reference spectrum, and integrated over 60 s to obtain total counts per spectrometer pixel. This waveguide Raman spectrum of toluene agrees well with the reference spectrum in Figure 4a, with two main differences. (i) The Raman peaks are broader for the waveguide measurement, due to the lower resolution of the system and (ii) there are additional Raman peaks in the waveguide spectrum at 677 and 928 cm^{-1} due to background emission.

The specified resolution of the commercial Raman instrument is ~1 cm^{-1} while the specified resolution of the compact spectrometer is ~5 cm^{-1}. Measurement of the scattered pump signal spectrum in the waveguide configuration shows that the estimated experimental resolution is ~58 cm^{-1}, with the discrepancy being due to bandwidth of the pump laser and the nature of collection by a highly multimode fibre. Specifically, the resolution is not high enough to resolve the two closely spaced peaks at 1,002 cm^{-1} and 1029 cm^{-1}. However, application to low-cost apparatus for detection and quantification of chemical species does not require

ultimate resolution and 58 cm^{-1} may be acceptable for field applications. The reduced spectral resolution of our system causes distortion of the spectra so that while Figure 4a (black trace) shows that the reference Raman peak at 1002 cm^{-1} is much higher than the peaks near 3000 cm^{-1}, Figure 4a (blue trace) shows the opposite for waveguide excitation. The reason for the apparent discrepancy is that the lines near 1000 cm^{-1} are much narrower than those near 3000 cm^{-1}, and so carry less power. To confirm the effect of the reduced resolution upon the measured spectra, the reference spectrum has been convolved with the spectral transfer function of the system (using the part of the collected spectrum corresponding to scattered pump radiation), and the resultant convolved reference spectrum is shown in Figure 4a (red trace). It is clear that the convolved spectrum (red trace) is very similar to the waveguide Raman spectrum (blue trace) in that the relative peak heights and linewidths are similar. This emphasises that the power carried by each line is a better measure of cross-section than the peak height.

The emission lines near 1000 cm^{-1} were selected for comparison of experimental measurements with the theoretical model and to determine the "power budget" for the system, in terms of power detected in a specific Raman line vs pump power launched into the waveguide, as the Raman cross-section for toluene at 1002 cm^{-1} is well-known [28]. Peaks were fitted to the experimental feature near 1,000 cm^{-1} using the Voigt function [30], as shown in Fig. 4b. The area confined under the red curve (1002 cm^{-1}) was then used to determine the total number of counts per 60 s due to the Raman line at 1002 cm^{-1} and then deduce the power in that line to be 2.11×10^{-15} W, with one spectrometer count at this wavelength (675.8 nm) corresponding to 7.2×10^{-18} J [31]. This corresponds to a conversion efficiency of 0.85×10^{-12} mm^{-1} (Watts of Raman power in the 1002 cm^{-1} line per Watt of pump power per mm of waveguide length, assuming that emission from 1 mm waveguide length is collected by the fibre).

4.2 Power budget.

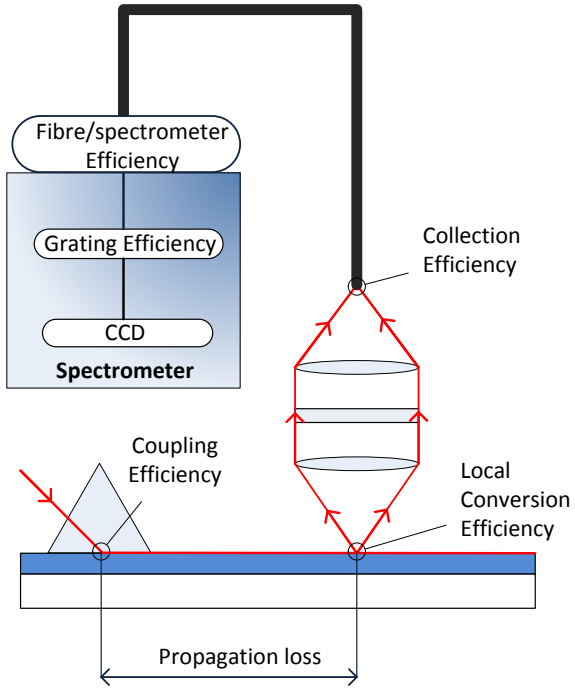

Figure 5. WERS system efficiency factors

Table I. Summary of efficiencies

Coupling efficiency (η_1)	0.30 ± 0.1
Propagation loss factor (η_2)	0.32 ± 0.1
Local conversion efficiency (η_3)	(7.0 ± 0.7) × 10^{-9}
Collection efficiency (η_4)	0.045 ± 0.005
Fibre/spectrometer efficiency (η_5)	0.02 ± 0.01
Grating efficiency (η_6)	0.60 ± 0.02
Total efficiency (η_T)	(3.6 ± 2.5) ×10^{-13}

A power budget analysis was performed in order to compare the experimental results with the simulations presented in Section 2 and to determine where improvements in the waveguide Raman system would provide a significant advantage. Figure 5 shows a schematic of the complete system with the major

efficiency factors indicated; the product of these efficiency factors results in a total conversion efficiency to compare with the experimental result obtained above. The estimated efficiency factors are given in Table 1, with the prism coupling efficiency, η_1, and the efficiency of pump propagation to the collection point, η_2, already discussed in Section 4.1.

The local conversion efficiency, η_3, relates the total Raman scattering at the waveguide surface to the pump power in the waveguide, over a specific collection area. The power emitted by a Raman line of a bulk material on a waveguide is given by the product of the number density of the emitting molecules, the Raman cross-section for that line and the pump intensity, over the excited volume. As only the intensity varies spatially and only in the x-direction (normal to the waveguide surface), this is given by:

$$P_e = \int \rho \cdot N_A/M \cdot A \cdot I(x) \cdot 4\pi \cdot d\sigma/d\Omega \cdot dx \qquad (2)$$

Where ρ and M are the density and molar mass of toluene, respectively, N_A is the Avogadro constant, A is the irradiated waveguide area covered by the bulk medium (D × L), I(x) is the pump intensity as a function of distance from the surface, $\frac{d\sigma}{d\Omega}$ is the differential Raman cross-section which, for isotropic radiation, yields a total cross-section of $4\pi \frac{d\sigma}{d\Omega}$. The term $\int I(x)\, dx$ is equal to the fractional power plotted in Fig 2, F_s, times the pump power per unit width in the waveguide, P_p/D. The conversion efficiency is then given by:

$$\eta_3 = P_e/P_p = \rho \cdot N_A/M \cdot 4\pi \cdot d\sigma/d\Omega \cdot F_s \cdot L \qquad (3)$$

In the case of our waveguide design for a superstrate medium with the refractive index of toluene, F_s is found to be 0.37, leading to a local conversion efficiency, η_3, of 8.2×10^{-6} per metre length of waveguide. In this experiment, a 0.85mm length of waveguide is imaged onto the 1 mm core of the fibre so that $\eta_3 = 7.0 \times 10^{-9}$.

As described in Section 2.2, the collection efficiency is determined by the numerical aperture of the collection system and the area from which the Raman scattering is collected, and is estimated here to be $\eta_4 \simeq 4.5\%$. The spectrometer has an intrinsic NA of 0.125 and a slit width of 200 μm. The combination of the reduced numerical and physical apertures yield an efficiency factor, $\eta_5 \simeq 2\%$ at the interface between the fibre and the spectrometer. The grating efficiency (η_6) is taken from the spectrometer datasheet to be 60% at the Raman scattering wavelength of 675.8 nm. Equation 4 then gives power arriving at the CCD, P_d, in terms of the incident pump power in the waveguide

$$P_d = P_i \cdot \eta_T = P_i \cdot \eta_1 \cdot \eta_2 \cdot \eta_3 \cdot \eta_4 \cdot \eta_5 \cdot \eta_6 \qquad (4)$$

resulting in a predicted power incident on the CCD array in the 1002 cm^{-1} Raman line of $(1.7 \pm 1.3) \times 10^{-14}\, W$ which is in reasonable agreement with the experimental result of $2.1 \times 10^{-15}\, W$ when it is considered that the analysis assumes isotropic Raman scattering and perfect optical alignment and that additional losses such as Fresnel reflections and fibre transmission losses have been ignored.

This power budget analysis has verified that the experimental power detected in a single Raman line from a simple bulk liquid analyte compares reasonably well with theoretical predictions, given experimental uncertainties. The efficiency factors which dictate the power budget make clear that the efficiency of transferring the emitted Raman power to the spectrometer CCD array is poor, but this is fundamentally limited by the brightness of the incoherent emission and the numerical and spatial apertures of the spectrometer. Collection of the Raman scattering in the waveguide is an attractive alternative as, for low-loss waveguides, collected power can be usefully built up over longer waveguide lengths but collection in

a monomode waveguide optimised for excitation by a (coherent) pump is normally poor leading to little advantage despite better aperture matching between the waveguide/spectrometer interface [12,32]. However, engineering the collection of surface Raman scattering at a waveguide surface by exploiting the non-isotropic nature of the emission is a promising avenue to explore [33].

To successfully repeat the experiment, it has been found out the waveguide sample should have a good guiding property, which can be indicated by a clean and long streak of light. The power confined by the waveguide needs to be checked in order to get detectable Raman signals. Providing that the laser power is fixed, the coupling efficiency may need to be optimised.

5. Conclusion

A theoretical and experimental analysis of waveguide-enhanced Raman spectroscopy (WERS) has been presented for the case of waveguide excitation and surface collection of Raman scattering, with explicit separation of the excitation and collection efficiencies. Raman signal enhancement factors of $>10^3$, compared with conventional Raman illumination, are predicted for surface spectroscopy on optimised high-contrast waveguides per millimetre waveguide length. Waveguides have been realised in thin tantalum pentoxide films and used to excite Raman scattering from toluene on the waveguide surface, which was detected with a low-cost spectrometer. A power budget analysis related the received power in a single Raman scattering line to the incident pump laser power, using waveguide surface intensity and Raman cross-section. Reasonable agreement has been obtained between theory and experiment for the received power in the 1002 cm^{-1} Raman line of toluene. This approach allows straightforward WERS optimization and a clear comparison of surface-enhanced techniques, and is expected to lead to low-cost, reproducible sensor systems for ultra-thin surface films without the complexity and variability associated with nanostructured plasmonic materials.

Acknowledgements

The authors would like to thank the European Research Council for funding this work under the European Union's Seventh Framework Programme (FP7/2007-2013) ERC grant agreement no. 291216 "Wideband Integrated Photonics for Accessible Biomedical Diagnostics". PNB gratefully acknowledges the receipt of a Wolfson Research Merit award.

References

[1] R.L. McCreery, Raman Spectroscopy for Chemical Analysis, John Wiley & Sons, Inc., Hoboken, NJ, USA, 2000. doi:10.1002/0471721646.

[2] P.L. Stiles, J.A. Dieringer, N.C. Shah, R.P. Van Duyne, Surface-enhanced Raman spectroscopy, Annu. Rev. Anal. Chem. (Palo Alto. Calif). 1 (2008) 601–26. doi:10.1146/annurev.anchem.1.031207.112814.

[3] S. Mahajan, J.J. Baumberg, A.E. Russell, P.N. Bartlett, Reproducible SERRS from structured gold surfaces, Phys. Chem. Chem. Phys. 9 (2007) 6016–6020. doi:10.1039/b712144j.

[4] K. Kneipp, K. Kneipp, H. Kneipp, H. Kneipp, I. Itzkan, I. Itzkan, et al., Ultrasensitive chemical analysis by Raman spectroscopy, Chem. Rev. 99 (1999) 2957–76. doi:10.1021/cr980133r.

[5] D. Cialla, A. März, R. Böhme, F. Theil, K. Weber, M. Schmitt, et al., Surface-enhanced Raman spectroscopy (SERS): Progress and trends, Anal. Bioanal. Chem. 403 (2012) 27–54. doi:10.1007/s00216-011-5631-x.

[6] M.E. Farrell, Targeting Biological Sensing with commercial SERS substrates, Adv. Environ. Chem. Biol. Sens. Technol. IX, Proc. SPIE. 8366 (2012).

[7] T. Hirschfeld, High-Sensitivity Attenuated Total-Reflection Spectroscopy, Appl. Spectrosc. 20 (1966) 336–338.

[8] J. Midwinter, On the use of optical waveguide techniques for internal reflection spectroscopy, IEEE J. Quantum Electron. 7 (1971). doi:10.1109/JQE.1971.1076805.

[9] J. Tschmelak, G. Proll, J. Riedt, J. Kaiser, P. Kraemmer, L. Bárzaga, et al., Automated Water Analyser Computer Supported System (AWACSS) Part I: Project objectives, basic technology, immunoassay development, software design and networking, Biosens. Bioelectron. 20 (2005) 1499–1508. doi:10.1016/j.bios.2004.07.032.

[10] C.A. Rowe, S.B. Scruggs, M.J. Feldstein, J.P. Golden, F.S. Ligler, An array immunosensor for simultaneous detection of clinical analytes, Anal. Chem. 71 (1999) 433–439. doi:10.1021/ac980798t.

[11] Y. Gu, S. Xu, H. Li, S. Wang, M. Cong, J.R. Lombardi, et al., Waveguide-enhanced surface plasmons for ultrasensitive SERS detection, J. Phys. Chem. Lett. 4 (2013) 3153–3157. doi:10.1021/jz401512k.

[12] A. Dhakal, A.Z. Subramanian, P. Wuytens, F. Peyskens, N. Le Thomas, R. Baets, Evanescent excitation and collection of spontaneous Raman spectra using silicon nitride nanophotonic waveguides, Opt. Lett. 39 (2014) 4025–4028.

[13] J.S. Kanger, C. Otto, M. Slotboom, J. Greve, Waveguide Raman Spectroscopy of Thin Polymer Layers and Monolayers of Biomolecules Using High Refractive Index Waveguides, J. Phys. Chem. 100 (1996) 3288–3292. doi:10.1021/jp952566t.

[14] Y. Levy, C. Imbert, J. Cipriani, S. Racine, R. Dupeyrat, Raman scattering of thin films as a waveguide, Opt. Commun. 11 (1974) 66–69. doi:10.1016/0030-4018(74)90336-8.

[15] J. Cipriani, S. Racine, R. Dupeyrat, H. Hasmonay, M. Dupeyrat, Y. Levy, et al., Raman scattering of Langmuir-Blodgett barium stearate layers using a total reflection method, Opt. Commun. 11 (1974) 70–73. doi:10.1016/0030-4018(74)90337-X.

[16] J.F. Rabolt, R. Santo, J.D. Swalen, Raman Spectroscopy of Thin Polymer Films Using Integrated Optical Techniques., Appl. Spectrosc. 33 (1979) 549–551. doi:10.1366/0003702794925101.

[17] J.F. Rabolt, N.E. Schlotter, J.D. Swalen, Spectroscopic studies of thin film polymer laminates using Raman spectroscopy and integrated optics, J. Phys. Chem. 85 (1981) 4141–4144. doi:10.1021/j150626a038.

[18] N. Schlotter, J. Rabolt, Raman spectroscopy in polymeric thin film optical waveguides. 1. Polarized measurements and orientational effects in two-dimensional films, J. Phys. Chem. 16 (1984) 2062–2067. doi:10.1021/j150654a025.

[19] J.F. Rabolt, R. Santo, N.E. Schlotter, J.D. Swalen, Integrated Optics and Raman Scattering: Molecular Orientation in Thin Polymer Films and Langmuir-Blodgett Monolayers, IBM J. Res. Dev. 26 (1982) 209–216. doi:10.1147/rd.262.0209.

[20] S. Ellahi, R.E. Hester, Enhanced waveguide Raman spectroscopy with thin films. Plenary lecture, Analyst. 119 (1994) 491. doi:10.1039/an9941900491.

[21] F. Peyskens, A. Subramanian, A. Dhakal, N. Le Thomas, R. Baets, Enhancement of Raman Scattering Efficiency by a Metallic Nano-antenna on Top of a High Index Contrast Waveguide, in: CLEO 2013, OSA, Washington, D.C., 2013: p. CM2F.5. doi:10.1364/CLEO_SI.2013.CM2F.5.

[22] D. Hu, Z. Qi, Refractive-Index-Enhanced Raman Spectroscopy and Absorptiometry of Ultrathin Film Overlaid on an Optical Waveguide, J. Phys. Chem. C. 117 (2013) 16175–16181. doi:10.1021/jp4052903.

[23] X. Jiang, L. Tang, J. Song, M. Li, J.-J. He, Integrated Raman spectroscopic sensor based on silicon nanowire waveguides, 9274 (2014) 92740I. doi:10.1117/12.2071446.

[24] C. Fu, Y. Gu, Z. Wu, Y. Wang, S. Xu, W. Xu, Surface-enhanced Raman scattering (SERS) biosensing based on nanoporous dielectric waveguide resonance, Sensors Actuators, B Chem. 201 (2014) 173–176. doi:10.1016/j.snb.2014.04.091.

[25] M.W. Meyer, K.J. McKee, V.H.T. Nguyen, E.A. Smith, Scanning Angle Plasmon Waveguide Resonance Raman Spectroscopy for the Analysis of Thin Polystyrene Films, J. Phys. Chem. C. 116 (2012) 24987–24992. doi:10.1021/jp308882w.

[26] Eric Le Ru and Pablo Etchegoin, Principles of Surface-Enhanced Raman Spectroscopy and related plasmonic effects, Elsevier, 2008.

[27] C.A. Burrus, Small-area high-radiance light-emitting diodes coupled to multimode optical fibers, in: Top. Meet. Integr. Opt. Waves, Mater. Devices, Las Vegas, NV, USA, 1972.

[28] K. Schmitt, K. Oehse, G. Sulz, C. Hoffmann, Evanescent field Sensors Based on Tantalum Pentoxide Waveguides – A Review, Sensors. 8 (2008) 711–738. doi:10.3390/s8020711.

[29] E.C. Le Ru, E.J. Blackie, M. Meyer, P.G. Etchegoin, Surface Enhanced Raman Scattering Enhancement Factors: A Comprehensive Study, J. Phys. Chem. C. 111 (2007) 13794–13803. doi:10.1021/jp0687908.

[30] M. Bradley, Curve Fitting in Raman and IR Spectroscopy : Basic Theory of Line Shapes and Applications, Thermo Fish. Sci. Appl. Note 50733. (2007) 0–3. http://thermo.fr/eThermo/CMA/PDFs/Product/productPDF_57565.PDF.

[31] Ocean Optics, QE65000 and Maya2000 Spectrometers, (n.d.). http://oceanoptics.com/wp-content/uploads/OEM-Data-Sheet-QE65000.pdf.

[32] D. Marcuse, Launching light into fiber cores from sources located in the cladding, J. Light. Technol. 6 (1988) 1273–1279. doi:10.1109/50.4130.

[33] C. Chen, J.-Y. Li, L. Wang, D.-F. Lu, Z.-M. Qi, Waveguide-coupled directional Raman radiation for surface analysis, Phys. Chem. Chem. Phys. (2015). doi:10.1039/C4CP05092D.